

Hyperbranched Fluoropolymer and Linear Poly(ethylene glycol) Based Amphiphilic Crosslinked Networks as Efficient Antifouling Coatings: An Insight into the Surface Compositions, Topographies, and Morphologies

CHAKRAVARTHY S. GUDIPATI,¹ C. MICHAEL GREENLIEF,² JEREMIAH A. JOHNSON,¹
PORNPIMOL PRAYONGPAN,² KAREN L. WOOLEY¹

¹Center for Materials Innovation and Department of Chemistry, Washington University, One Brookings Drive, Saint Louis, Missouri 63130-4899

²Department of Chemistry, University of Missouri–Columbia, 601 South College Avenue, Columbia, Missouri 65211-7600

Received 16 June 2004; accepted 5 August 2004

DOI: 10.1002/pola.20466

Published online in Wiley InterScience (www.interscience.wiley.com).

ABSTRACT: Polymer coatings with features of differing hydrophilicity, mobility, and topography, distributed across a substrate in microscopic and nanoscopic patches were designed as complex materials equipped with sufficient variability in composition, structure, and dynamics to inhibit interactions associated with biomacromolecular fouling. These complex polymer coatings were prepared by the in situ phase separation and crosslinking of mixtures of hyperbranched fluoropolymer (HBFP) and diamino-terminated poly(ethylene glycol) (PEG), for which the degree of crosslinking, compositions, topographies, and morphologies were varied by alteration of the PEG/HBFP stoichiometries (14, 29, 45, and 55 wt % PEG). This article examines the physicochemical details of HBFP–PEG network coatings prepared on glass substrates, functionalized by 3-aminopropyltriethoxysilane, as characterized by atomic force microscopy (AFM), contact-angle measurements, X-ray photoelectron spectroscopy (XPS), differential scanning calorimetry (DSC), and thermogravimetric analysis. Upon incubation in water or artificial seawater, the surfaces underwent reconstruction, which was believed to be driven by the swelling of the PEG domains and the energetic favorability offered by the segregation of PEG to the solid–water interface. © 2004 Wiley Periodicals, Inc. *J Polym Sci Part A: Polym Chem* 42: 6193–6208, 2004

Keywords: hyperbranched polymers; amphiphiles; crosslinking; fluoropolymers; poly(ethylene glycol)

INTRODUCTION

Fluoropolymers^{1–14} have been the focus of extensive research in the development of minimally adhesive surfaces because of their low surface energy, low wettability, and chemical stability,

which have also led to studies of their utility as potential antifouling materials for marine applications,^{15–20} among other things.^{21–24} It has been established that fouling by marine organisms upon surfaces such as ship hulls involves a process by which the organism secretes an adhesive protein or glycoprotein, either of a hydrophobic²⁵ or hydrophilic nature,^{26,27} depending on the fouling species, that provides for binding to the surface through various modes of interaction, including chemical bonding, electrostatic interaction,

Correspondence to: K. L. Wooley (E-mail: klwooley@artsci.wustl.edu)

Journal of Polymer Science: Part A: Polymer Chemistry, Vol. 42, 6193–6208 (2004)
© 2004 Wiley Periodicals, Inc.

diffusion, and mechanical interlocking.²⁸ In this regard, it becomes imperative that any coating formulated for preventing both soft and hard fouling present a surface that can simultaneously defeat all the modes of interaction between the fouling organism and the surface.

The development of synthetic materials that inhibit protein adsorption has received considerable attention, and effective materials have been realized^{29–34}; however, the marine fouling problem goes beyond limiting interactions with proteins, and the surface features must be of increased complexity to account for the various modalities for marine organism attachment and the dimensions over which they occur. Although the chemical and electrostatic interactions between the surface and the fouling organism may be minimized by morphologically and compositionally heterogeneous surface patterns, the diffusion and mechanical interlocking modes of interaction may be defeated by surface topographical complexities coupled with the necessary mechanical integrity of the coating. In addition, molecular-level topology has also been demonstrated to be an important parameter in providing control over protein adsorption. Nienhaus et al.³⁵ reported recently the ability of surfaces, consisting of isocyanato-terminated star-shaped poly(ethylene oxide-co-propylene oxide) molecules crosslinked via urea linkages upon partial hydrolysis under an ambient atmosphere, to inhibit nonspecific protein adsorption and to allow for protein renaturation, whereas poly(ethylene oxide) (PEO) brush surfaces allowed for irreversible protein denaturation, which was believed to occur through the intermingling of the polypeptide chains with the linear PEO brushes.

Our strategy for the preparation of robust, crosslinked networks of polymer materials that present complex surface morphologies and topographies relies upon controlling the molecular topology and is based on the *in situ* crosslinking of phase-segregating mixtures of incompatible polymer precursors. This process relies on the thermodynamically driven phase segregation of hydrophilic poly(ethylene glycol) (PEG) and hydrophobic hyperbranched fluoropolymers (HBFPs), which is kinetically trapped by the reaction of amino termini present on each of the two chain ends of PEG and pentafluorophenyl groups that reside in large numbers as the chain termini of the hyperbranched architecture.^{36–38} Copolymerization with fluorinated monomers to tune the properties of polymers has been used in many

examples,^{39,40} and the strategy of using phase segregation in copolymers, especially those containing fluorinated blocks,^{8,41–43} to prepare surfaces with ordered morphologies is well known.¹ Moreover, there exist many examples of hybrid linear–dendritic block copolymers,^{44–46} as well as dendritic or hyperbranched polymers, modified via coupling with PEO into amphiphilic star structures^{47–50} that undergo interesting solution-state,⁵¹ surface,⁵² and bulk microphase segregation⁵³ or modified via the crosslinking of the branched macromolecules with PEG^{54,55} into amphiphilic matrices as interpenetrating networks that contain domains rich in each of the components.^{56,57} Interestingly, semifluorinated monodendron surface-active block copolymers⁵⁸ and other fluorinated block copolymers⁵⁹ have been shown to undergo microphase segregation and surface reorganization to provide for a dynamic presentation of surface composition, topography, and morphology.

Coupled with the well-known resistance of PEG surfaces toward protein adsorption and bacterial adhesion,^{32,60–62} the coatings of crosslinked HBFP–PEG networks are designed to exhibit varying wettability and hydrophobicity, the factors that have been shown to impart resistance toward biofouling.^{29,63,64} Previous work has demonstrated that the crosslinking of HBFP and PEG generates surfaces of compositionally variant, nanoscopically resolved morphologies and topographies, along with improved mechanical integrity.⁵⁶ The dimensions of the topographical features, which could be tuned to a scale comparable to that of marine adhesive biomacromolecules, were shown to be controlled by the HBFP–PEG stoichiometry and the coating thickness. However, all of the coatings studied previously were prepared by the spin coating of HBFP and PEG mixtures onto mica, which produced ultrathin coatings that were not well attached to the substrate. In this article, we report the preparation of coatings with thicknesses of several micrometers on glass substrates, with covalent attachment between the HBFP–PEG network and the glass. The surface features of these materials were characterized by X-ray photoelectron spectroscopy (XPS), static contact-angle measurements, and atomic force microscopy (AFM), and the thermal properties were evaluated with differential scanning calorimetry (DSC) and thermogravimetric analysis (TGA). A highly interesting surface reorganization phenomenon was observed for these amphiphilic materials upon treatment

with water or an organic swelling agent, and the reversibility of this process was evaluated.

EXPERIMENTAL

Materials

Diisopropylethylamine (DIEA), 3-aminopropyltriethoxysilane (3-APS), bis(3-aminopropyl)-terminated PEG [number-average molecular weight (M_n) = 1600 Da and number-average degree of polymerization (DP_n) = 34], and all solvents were purchased from Aldrich Chemical Co. and were used as received. The diglycidyl ether of PEG (M_n = 3000) was obtained from Scientific Polymer Products. Chloroform and methanol were used as purchased, whereas tetrahydrofuran (THF) was distilled from Na. The artificial seawater used for the incubation of the polymer coatings was a Coralife scientific-grade marine salt solution in deionized (DI) water at a concentration of 0.3 lb/gal. HBFPs (**1**) were synthesized according to a procedure previously reported.³⁶ HBFP **1a** [M_n = 9700 Da, DP_n = 20, and weight-average molecular weight/number-average molecular weight (M_w/M_n) = 1.8] was used in the XPS experiments, and **1b** (M_n = 9200 Da, DP_n = 19, and M_w/M_n = 2.4) was used in the preparation of the crosslinked HBFP-PEG coatings for AFM and contact-angle measurements, whereas **1c** (M_n = 7900, DP_n = 16, and M_w/M_n = 2.2) was used in the preparation of HBFP-PEG coatings for DSC and TGA.

General Procedure for the Preparation of HBFPs Crosslinked with Bis(3-aminopropyl)-Terminated Poly(ethylene glycol) (**2**)

The crosslinked HBFP-PEG networks were prepared according to the procedure previously reported as method II,⁵⁶ in which the HBFP, PEG, and DIEA were dissolved in THF and the solution was heated at reflux for 20 h under nitrogen. This yielded products with characterization data in agreement with those reported. The solutions were then used for coating the functionalized glass microscope slides.

General Procedure for the Preparation of Coatings on Microscope Glass Slides

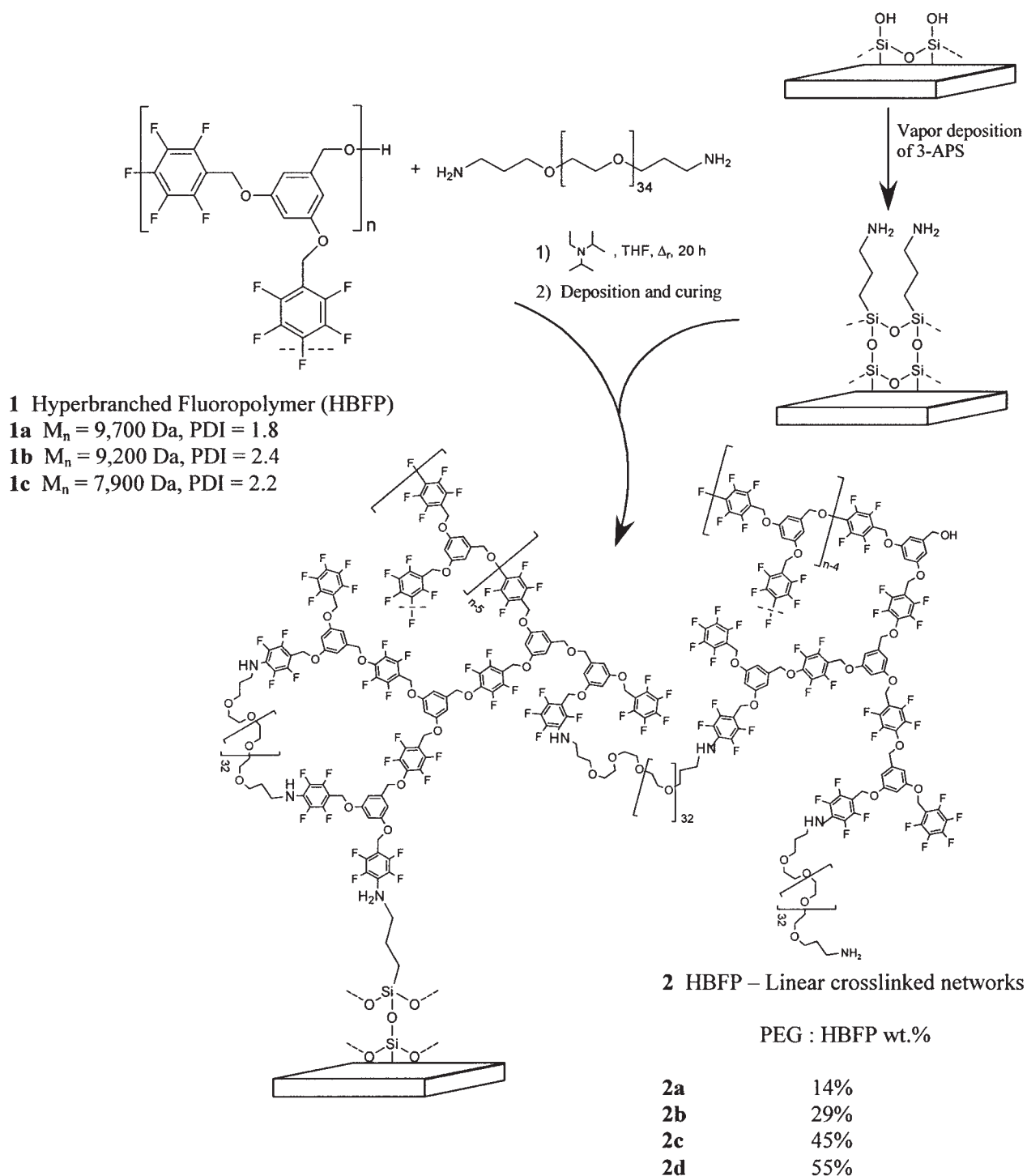
The microscope glass slides (Fisher Scientific; 75 × 25 × 1 mm³) were cleaned in a CHCl₃/

methanol (50:50) solvent mixture in an ultrasonic cleaner for 30 min and were dried *in vacuo* at room temperature in a desiccator for 1 h. The slides were typically stored under nitrogen for 30 min, and then 3-APS (300 μL) was added to allow for functionalization by vapor deposition at room temperature under nitrogen for 2 h.⁶⁵ The slides were then coated by multiple cycles of immersion into a THF solution containing DIEA, HBFP, and PEG-(NH₂)₂ for **2a**, **2b**, **2c**, and **2d** (with 14, 29, 45, and 55 PEG wt %, respectively) or into a solution of HBFP in THF (5% w/v) for **1a**, **1b**, and **1c** (differing in the HBFP sample molecular weight; see Scheme 1) with intermediate drying. The glass slides were then heated at 100 °C for 1 h under nitrogen. PEG-grafted glass surfaces were prepared by the immersion of the 3-APS-functionalized glass substrates in a 10% (w/v) solution of diglycidyl ether of PEG (M_n = 3000) in a sodium phosphate buffer (0.05 M NaH₂PO₄-Na₂HPO₄, 0.15 M NaCl, and pH 7.3) for 6 h at 60 °C.⁶⁶ All the coatings were pale yellow upon curing. The coatings were used as prepared for contact-angle, AFM, and XPS experiments. For the DSC and TGA experiments, films scratched from the substrate were used as samples.

Measurements

IR spectra were obtained with a Mattson Polaris spectrometer for samples in the form of thin films on KBr disks. ¹⁹F NMR spectra were recorded at 282.2 MHz for solutions in CDCl₃ on a Varian Mercury 300 spectrometer, with CFCl₃ as the external reference. Contact angles were measured as static contact angles by the standard sessile drop technique with a TanteC CAM micro contact-angle meter and the half-angle measuring method. Film thicknesses were measured with Tencor Instruments Alpha-Step 200 equipment. Contact angles of nanopure water (17.8 MΩ cm, 4 μL) were measured on films approximately 30 s after the drop application. The reported values are averages of five measurements from different regions of the same sample surface.

DSC was performed on a Mettler-Toledo instrument with the DSC822^e module, calibrated with an indium standard. The data were analyzed with STAR^e SW 7.01 software. The coatings of the crosslinked HBFP-PEG materials were scratched from the substrate, and 3–5 mg was used for the DSC measurements. For DSC of crosslinked HBFP-PEG materials swollen with water, the



Scheme 1. Preparation of the crosslinked HBFP–PEG networks and the covalent attachment of the coatings to 3-APS-functionalized glass microscope slides.

samples (3–5 mg) were weighed into an aluminum pan, and a known amount of water (30–40 wt %) was added; the samples were allowed to equilibrate for 30 min. The samples of dry and

swollen crosslinked materials were heated and cooled between -50 and 150 °C at a rate of 10 °C/min in three repetitions of heating–cooling cycles. The glass-transition temperatures (T_g 's) were

measured as the midpoint of the inflection tangent upon the third or subsequent heating scans. The melting temperatures (T_m 's) were measured as the onset of the melting endotherms.

The XPS measurements for the HBFP, PEG, and crosslinked HBFP-PEG network coatings were collected to examine the compositions of the polymer surfaces before and after incubation in water. A VSW twin X-ray source was used in this study. X-ray photoelectron spectra were taken with Al K α radiation (1486.7 eV), with the anode operating at 300 W. A cylindrical mirror analyzer (model 15-255GAR, Physical Electronics, Inc.) was operated at a fixed pass energy of 25 eV. For each sample, F(1s), O(1s), C(1s), and Si(2p) core-level spectra were collected, and nonlinear curve fitting software was used for data analysis. The spectra were fit to the sums of Lorentzian and Gaussian line shapes. Through peak fitting, the components associated with different surface-bonded species in the spectra were identified. The 3-APS-functionalized glass microscope slides were coated with the HBFP, PEG, and crosslinked HBFP-PEG through dip coating into the corresponding solutions in THF. For studying the effect of the water treatment on the surface composition, the samples were incubated in DI water, and this was followed by drying at 60 °C *in vacuo* for 12 h. The shifts in the binding energies in the C(1s) region in each of the samples due to surface charging were corrected by all the C(1s) component peaks being referenced to the saturated C binding energy of 285.0 eV. All the samples were found to contain Si contaminants (2–8%) at the surface, and rinsing with THF before the experiments did not reduce the contamination level.

TGA was conducted on a Mettler-Toledo instrument with a TGA/SDTA851^e module, and the data were analyzed with STAR^e SW 7.01 software. The samples were heated from 0 to 600 °C at a rate of 10 °C/min. The onset temperature for weight loss was the point at which two tangential lines in the TGA curves intersected.

AFM experiments were performed with a Nanoscope III scanning probe microscope from Digital Instruments. The surface morphologies and topographies were investigated in the tapping mode with a Digital Instruments Bioscope instrument (dimension head and G scanner) under ambient conditions, with a silicon tip (160 μm , 325 kHz) with a nominal spring constant of 40 N/m. After the analysis of the dry films, the slides were incubated in artificial sea-

water for 1 day; this was followed by rinsing with DI water and drying *in vacuo* at the ambient temperature for 1 day. After incubation in artificial seawater, the films were thoroughly rinsed with DI water to make sure that the components of the seawater did not influence the surface chemistry.

RESULTS AND DISCUSSION

Synthesis

Amphiphilic hyperbranched-linear copolymer networks were generated from HBFP (**1**) and bis(3-aminopropyl)-terminated PEG. The HBFP, with a 50% statistical degree of branching and an average of one pentafluorophenyl group per repeat unit, was synthesized from an AB₂ monomer, 3,5-bis(pentafluorobenzyloxy)benzyl alcohol, by condensation polymerization according to a procedure previously reported.³⁶ HBFPs from batches of slightly different molecular weights (**1a–1c**) were used in this study, simply because of availability. There were no apparent differences in the network materials resulting from these three different precursors. The *para*-fluorines of the pentafluorophenyl end groups of the HBFP were reactive and provided a mechanism for intramolecular or intermolecular crosslinking of the HBFP via nucleophilic aromatic substitution by the amine termini of the PEG (Scheme 1). Variations in the degree of crosslinking could be achieved by the alteration of the stoichiometry of PEG with respect to the HBFP, which in turn provided a means of manipulating the compositional, morphological, and topographical features, as observed for thin films of crosslinked HBFP-PEG networks.⁵⁶

Crosslinked networks were produced from mixtures of HBFP and diamino-terminated PEG at 14, 29, 45, and 55 wt % PEG/HBFP. Solutions of HBFP, diamino-PEG, and DIEA in THF were allowed to form pregel structures by being heated at reflux for 20 h and were then deposited onto glass substrates and cured at 100 °C. Monitoring the solution-state precuring reaction by ¹⁹F NMR spectroscopy indicated that the extent of substitution of *para*-fluorines, as determined by the relative decrease in the corresponding ¹⁹F resonance at -153.5 ppm, was approximately 20% for **2c** and **2d**, whereas it was indiscernible for **2a** and **2b**. As noted in a previous work,⁵⁶ the pre-establishment of stars and higher crosslinked aggregates before the reaction mixture is drawn onto

the glass substrate gives enhanced gel formation, by which the crosslinking chemistry continues during the curing process at an elevated temperature and upon solvent evaporation, with the phase segregation being limited in domain sizes.

Microscope glass slides functionalized with 3-APS were used as substrates for preparing thick films of HBFP–PEG crosslinked materials through multiple dip coating into THF solutions containing HBFP, diamino-terminated PEG, and DIEA and were precured as discussed previously. Initial attempts at coating nonfunctionalized glass slides resulted in unstable films that delaminated upon incubation in water. To prevent the delamination of the coated material, the glass surface was treated with 3-APS according to protocols that were previously reported⁶⁵ for the surface modification of mica. The chemical vapor deposition of 3-APS under nitrogen resulted in amine groups on the surfaces of the glass slides, which provided covalent attachment points for the HBFP by the nucleophilic substitution of the *para*-fluorines of the pentafluorophenyl end groups of the HBFP (Scheme 1). This process effectively affixed the entire network coating to the substrate. Coatings prepared on the functionalized slides did not delaminate in water or artificial seawater. Coatings of pure HBFP were prepared through the immersion of 3-APS-functionalized glass slides into a solution of HBFP in THF (5% w/v) followed by curing at 100 °C under nitrogen; this resulted in the covalent attachment of the polymer to the substrate, which prevented delamination. The PEG was grafted onto the glass substrate according to the protocol reported in the literature.⁶⁶

The thickness values for the coatings prepared via dip coating on 3-APS-functionalized glass slides were determined by Alpha-Step measurements, and the data are summarized in Table 1. The thicknesses of the coatings increased with increasing PEG content, from 0.55 μm for the neat HBFP to 0.67, 0.91, 1.04, and 6.29 μm for the crosslinked HBFP–PEG networks as the amount of PEG was increased from 14 to 29 to 45 to 55%, respectively (Table 1).

Surface Wettability and Composition

The static contact angles of water on the crosslinked HBFP–PEG coatings and poly(tetrafluoroethylene) (PTFE; used as a control sample) were measured by the sessile drop technique. The contact angle of water on the HBFP surface revealed its highly hydrophobic nature, similar to that of PTFE. The XPS spectrum of the HBFP coating (Fig. 1) revealed F(1s), C(1s), and O(1s) peaks, suggesting the orientation of the low-surface-energy pentafluorophenyl end groups at the polymer–air interface, which imparted the high degree of hydrophobicity to the surface. On the other hand, the contact-angle values for the crosslinked HBFP–PEG network coatings, summarized in Table 1, exhibited a gradual descent as the PEG composition in the crosslinked HBFP–PEG networks was increased from 14 to 29 to 45 to 55 wt %. The observed trend indicated that the relative composition of PEG versus HBFP at the polymer–air interface increased with an increasing PEG weight percentage in the crosslinked network. A similar direct correlation between the surface and bulk compositions of the PEG segments was observed before.^{67,68}

Table 1. Static Contact Angles of Water on the Crosslinked HBFP–PEG Coatings, Measured before and after Incubation in Artificial Seawater^a

Polymer	PEG (wt %)	Film Thickness (μm) ^b	Angle before Incubation in Artificial Seawater	Angle after Incubation in Artificial Seawater
PTFE	—	—	110.4 \pm 2.0°	— ^c
1b	0	0.55 \pm 0.08	89.0 \pm 2.0°	— ^c
2a	14	0.67 \pm 0.08	74.5 \pm 4.0°	67.5 \pm 2.0°
2b	29	0.91 \pm 0.08	68.5 \pm 3.0°	60.5 \pm 2.0°
2c	45	1.04 \pm 0.15	61.0 \pm 3.0°	54.0 \pm 1.0°
2d	55	6.29 \pm 1.42	54.5 \pm 5.0°	48.5 \pm 2.0°
PEG	100	— ^a	25.3 \pm 3.0°	— ^d

^a The decrease in the contact angle, after incubation in water, indicates reorientation of the surface leading to increased hydrophilicity. The HBFP (**1b**) was used in the preparation of the HBFP–PEG crosslinked networks.

^b Thickness of the dry coatings, as measured by the Alpha-Step instrument.

^c Data not obtained.

^d An observable value could not be obtained because of wetting.

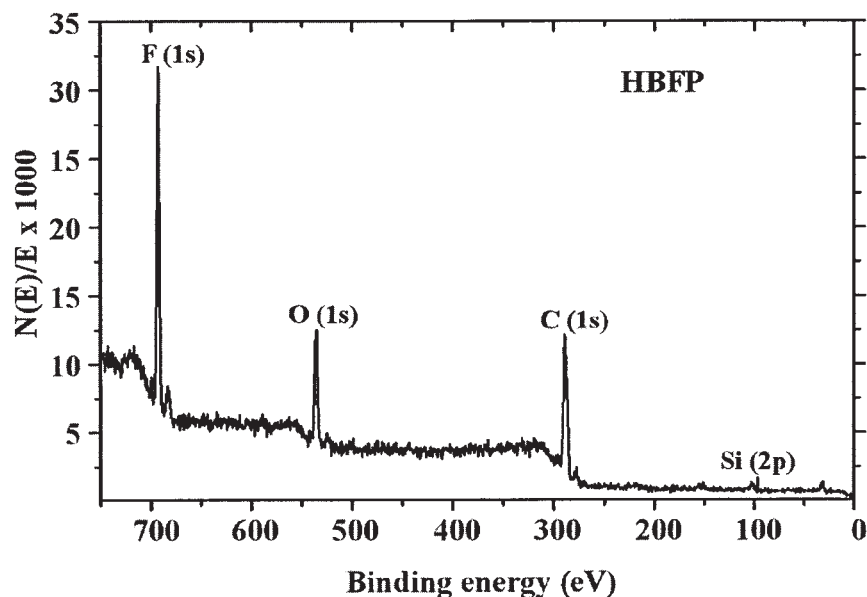


Figure 1. X-ray photoelectron wide-scan survey spectrum of an HBFP coating prepared on a 3-APS-functionalized microscope glass slide. The F(1s), C(1s), and O(1s) peaks in the spectrum indicate the orientation of the low-surface-energy pentafluorophenyl groups at the polymer–air interface. HBFP **1a** was used in the preparation of the crosslinked HBFP–PEG materials in the XPS experiments.

The atomic concentrations of the surface elements in each of the crosslinked HBFP–PEG coatings, determined by XPS and summarized in Table 2, demonstrated a decline in the relative concentrations of fluorine and a gradual increase in the carbon and oxygen concentrations from **2a** to **2d**, in agreement with the surface and bulk compositions of the PEG segment. Upon incubation in artificial seawater or pure DI water for 1 day followed by drying, each of the crosslinked HBFP–PEG network coatings exhibited lower contact angles with water than those on the respective coatings before seawater incubation (Table 1). The increase in the surface hydrophilicity of the coatings, upon incubation in water, was presumably a corollary of surface reconstruction, which resulted in the PEG domains preferentially aligning themselves at the polymer–water interface to minimize the interfacial tension. Similar observations involving the reorientation of amphiphilic copolymer surfaces upon contact with water, resulting in changes in the surface hydrophilicity, were previously reported, examples of which include crosslinked HBFP–PEG materials^{56,69} and poly(methyl methacrylate)-*g*-poly(dimethylsiloxane) copolymer surfaces.

This surface reorganization process is very well manifested in a plot of the fluorine/carbon atomic

concentration ratios as a function of the PEG weight percentage (Fig. 2). The fluorine content decreased as the amount of PEG segregating to the surface increased, and this was in turn a function of the PEG content in the network. Treatment with water induced further mobility in the PEG domains, which migrated to the polymer–water interface to maximize the interaction with water. The extent to which the migration took place was largely dependent on the relative amounts of PEG chains at the polymer–air/polymer–water interfaces and those inside the matrix. For **2a** (Fig. 2), the F/C ratio before and after incubation in water did not change considerably because of smaller PEG domains, which restricted the chain movement, whereas the PEG domains in network coating **2b** were large enough to cause migration to the polymer–water interface upon contact with water, and this resulted in a drastic reduction of the F/C ratio. A considerable decrease in the F/C ratio was also observed for **2c**, whereas **2d** exhibited a diminished difference in the F/C ratio after water treatment, presumably because of the presence of a significant amount of PEG at the polymer–air interface before the water treatment, even though it was believed that both HBFP and PEG domains were interspersed throughout the network coating.

Table 2. Surface Atomic Concentrations of the HBFP, Diamine-Terminated PEG, and Crosslinked HBFP-PEG Films, Determined by XPS^a

Coating	PEG (wt %)	Dry Coating			After Water Incubation		
		F(1s)	O(1s)	C(1s)	F(1s)	O(1s)	C(1s)
1a	0	0.139	0.174	0.621	— ^b	— ^b	— ^b
2a	14	0.105	0.189	0.612	0.140	0.178	0.672
2b	29	0.120	0.041	0.767	0.082	0.181	0.687
2c	45	0.063	0.140	0.564	0.063	0.222	0.638
2d	55	0.029	0.229	0.653	0.034	0.235	0.673
PEG	100	—	0.204	0.976	— ^b	— ^b	— ^b

^a The HBFP (**1a**) was used in the preparation of the crosslinked HBFP-PEG materials for the XPS experiments.

^b Data not obtained.

A detailed investigation of the C(1s) core-level region revealed three component peaks emanating because of C—H, C—O and C—F binding energies at 286.8, 288.2, and 289.5 eV, respectively (Table 3), providing further insight into the relative concentrations of HBFP versus PEG at

the surface. Because there was a possibility that the peak positions might shift because of surface charging upon prolonged exposure to X-rays, all the component C(1s) peaks were referenced to the saturated C binding energy of 285.0 eV. At lower PEG weight percentages (14 and 29%), the C—F

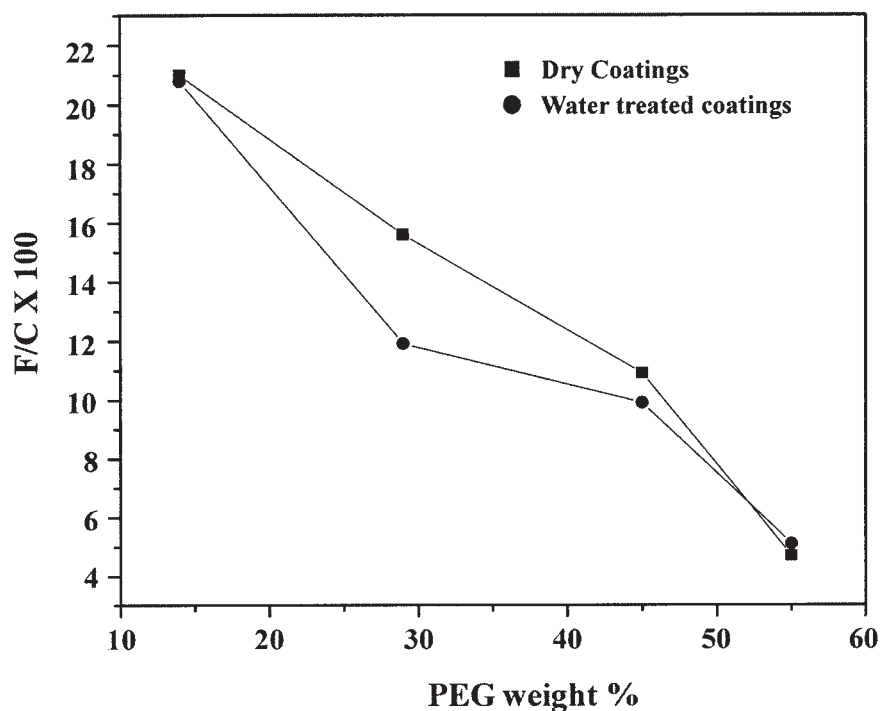


Figure 2. Comparison of the ratios of the fluorine atomic concentration to the carbon atomic concentration on the surfaces of crosslinked HBFP-PEG network coatings, before and after incubation in water. The F/C ratios indicate increased segregation of PEG at the polymer-air or polymer-water interface with an increase in the PEG weight percentage and upon treatment with water, respectively. HBFP **1a** was used in the preparation of the crosslinked HBFP-PEG materials in the XPS experiments.

Table 3. Percentage Areas of the Component Peaks in the C(1s) Core-Level Region of the HBFP, Diamine-Terminated PEG, and Crosslinked HBFP-PEG Network Coatings, Determined by XPS^a

Coating	Dry coating			After Incubation in Water		
	C-H	C-O	C-F	C-H	C-O	C-F
1a	35.57	17.28	47.15	—	—	—
PEG-(NH ₂) ₂	13.86	85.69	—	—	—	—
2a	49.45	15.38	34.53	42.02	42.37	13.39
2b	35.11	40.80	22.50	37.91	29.57	31.61
2c	34.37	52.46	12.29	42.48	51.71	5.82
2d	31.12	51.88	16.76	29.43	53.36	17.21

^a The HBFP (**1a**) was used in the preparation of the crosslinked HBFP-PEG materials for the XPS experiments. The contribution from C-F appears dominant at lower PEG concentrations, whereas C-O contribution becomes dominant at higher PEG compositions, before and after water treatment; this indicates the linear dependence of the surface PEG content on the bulk concentration.

peak was dominant, whereas at higher PEG concentrations (45 and 55%), the C—O peak dominated, as implied by the percentage peak areas of the C(1s) component peaks shown in Table 3. However, the decrease in the percentage peak area of the C—F peak for the **2c** coating upon incubation in water was much greater than that for **2d**, suggesting the extent to which the PEG in **2d** coating segregated to the polymer-air interface even before water treatment.

Surface Topography

Tapping-mode AFM was used to evaluate the topographical features of the crosslinked HBFP-PEG coatings. The images (Fig. 3) indicated the formation of complex domains that resulted from the thermodynamically induced phase segregation of the HBFP and PEG segments because of mutual incompatibility. The strategy of using the phase-separation behavior of fluorinated block copolymers and blends to generate highly ordered surfaces with liquid-crystalline properties^{70,71} and fouling-resistant characteristics⁷² is well known. The dimensions of the phase-segregated domains were largely dependent on the relative compositions of the individual blocks as well as the film thicknesses. In comparison, the AFM images of glass slides and 3-APS-treated glass slides were unremarkable (data not shown). As shown in Figure 3, the surface features of the **2a**, **2b**, and **2c** coatings were submicrometer in scale and increased in size with an increase in the amount of diamino-terminated PEG, whereas **2d** did not ex-

hibit discrete domains, possibly because of the higher segregation of PEG to the surface leading to the formation of a layer that was predominantly composed of PEG, with the HBFP segment being embedded underneath the matrix.

The surface reorganization resulting upon contact with artificial seawater or pure DI water and confirmed by contact-angle measurements as well as XPS analysis is also reflected in the AFM images. As shown in Figure 4, AFM imaging reveals the surface inversion from a morphology represented by peaks to a morphology represented by interconnected rings. In combination with the contact-angle and XPS data, we hypothesized that the initially prepared peaks consisted predominantly of HBFP and that the interconnected rings were predominantly composed of PEG segments.

Even though each coating appeared to undergo surface reconstruction, as shown by the decrease in the contact-angle values of water (Table 1) as well as the F/C ratios upon treatment with water (Fig. 2), the process, in terms of surface topography, was well pronounced for **2c** with a PEG weight percentage of 45% and, to a lesser extent, for **2b** with 29 wt % PEG, in comparison with **2a** and **2d** with PEG weight percentages of 14 and 55%, respectively. This was possibly due to a higher HBFP content for **2a** that resulted in smaller PEG domains, which were limited in flexibility, undergoing reorganization that was not resolvable on the scale of the experiments. Similarly, for **2d**, the surface was already rich in PEG segments, and so reconstruction upon water ex-

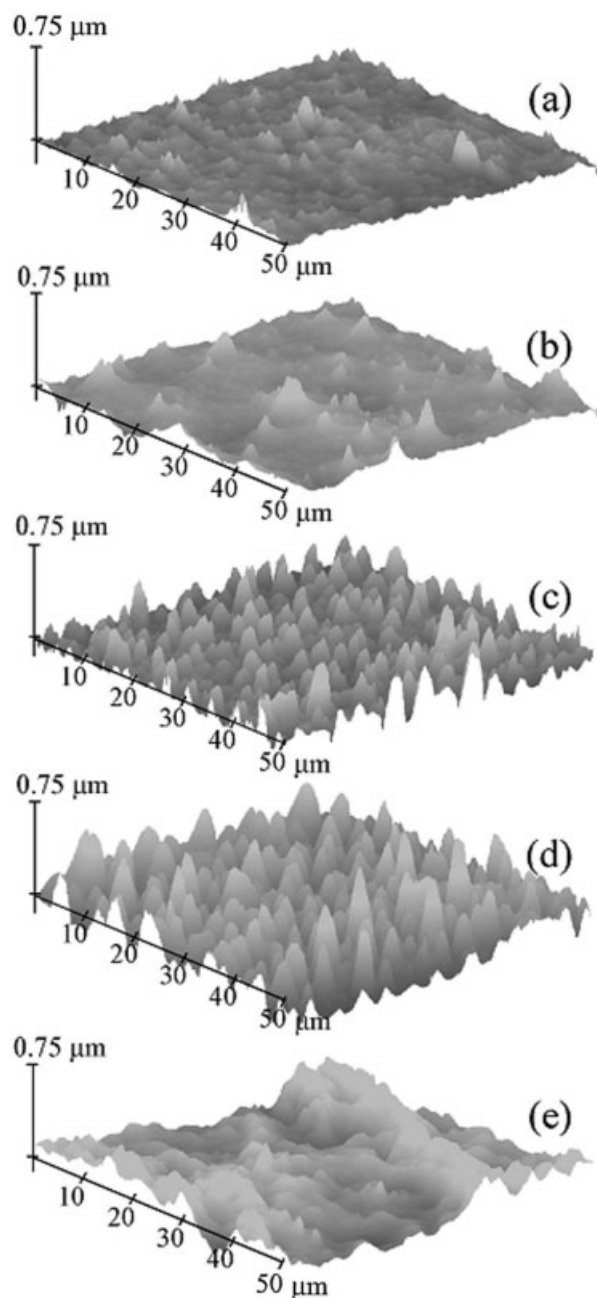


Figure 3. Tapping-mode AFM images of (a) **1b**, (b) **2a**, (c) **2b**, (d) **2c**, and (e) **2d** (prepared from **1b**). The topographical features increase in size as the PEG weight increases from 0 to 14 to 29 to 45 to 55%, respectively.

posure was not significant enough to be observable.

The surface reorganization was found to be a reversible process, which required the application of domain-selective solvents to accomplish reversibility. As illustrated in Figure 5, the inverted

surface [Fig. 5(b–d)], produced by the application of water to the initial 45 wt % PEG/HBFP coating [Fig. 5(a)], was stable to heating at 80 °C for 4 h and also upon drying at 60 °C for 12 h *in vacuo*. However, the application of a drop of THF resulted in the surface reverting to the original conformation [Fig. 5(e)], which was composed of HBFP-rich domains at the polymer–air interface and was similar to that of the dry virgin coating. The reintroduction of water to the THF-treated surface resulted in the migration of PEG-rich regions to the surface again.

Thermal Properties

DSC experiments were performed to evaluate the thermal properties of the crosslinked HBFP–PEG

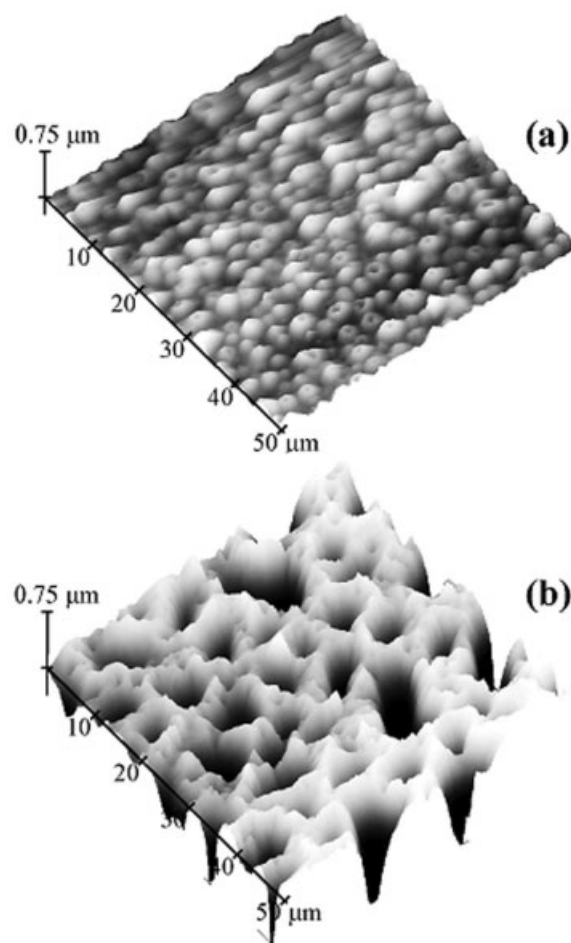


Figure 4. Tapping-mode AFM images of (a) **2b** and (b) **2c** after incubation in artificial seawater for 1 day and drying. The surface reorganization is more pronounced for **2c**, with 45 wt % PEG, than for any other coating.

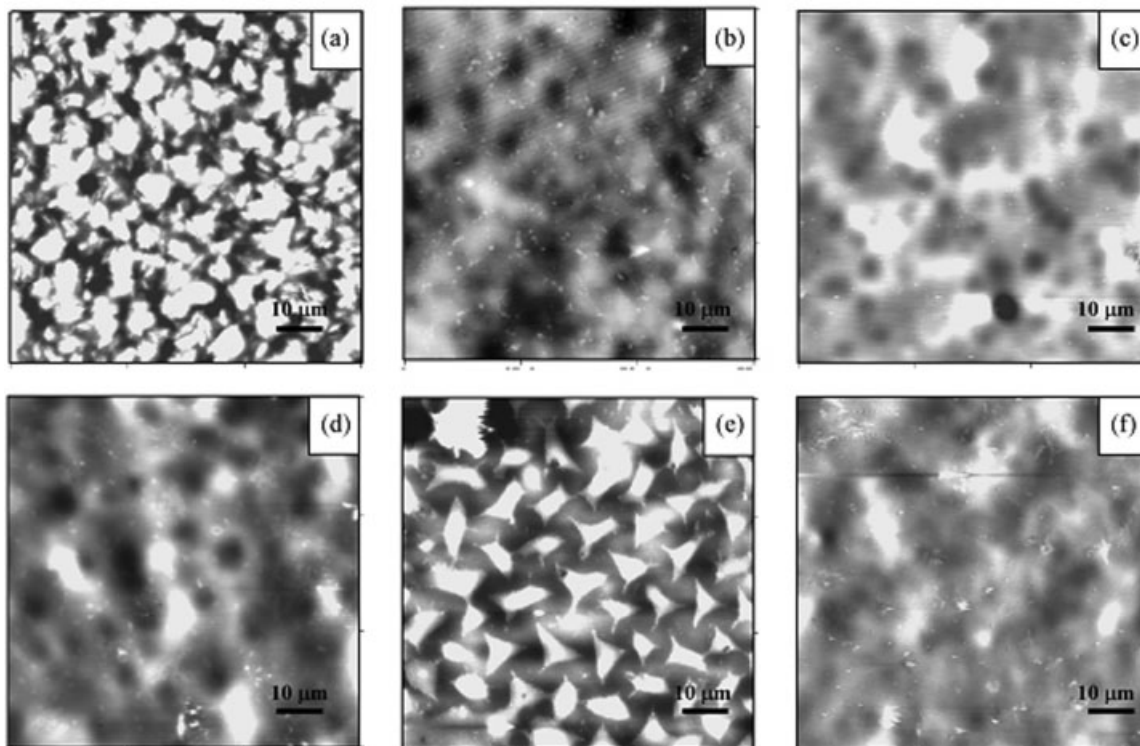


Figure 5. Tapping-mode AFM images of **2b** (prepared from **1b**) with 45 wt % PEG: (a) without treatment (as a pristine coating); (b) after water treatment for 15 min by the application of a 2- μ L drop of water, which absorbed the subsurface; (c) after heating at 80 $^{\circ}$ C for 4 h; (d) after drying further at 60 $^{\circ}$ C *in vacuo* for 12 h; (e) after a THF treatment for 15 min through the addition of a 2- μ L drop of THF, which absorbed the subsurface; and (f) after water treatment for 15 min and drying at 60 $^{\circ}$ C *in vacuo* for 12 h. Each of the images shows a 75 μ m \times 75 μ m area, with the height scale being 150 nm. The AFM images are shaded according to the height (z axis), and so the taller features are lighter, and the shorter features are darker.

Table 4. Thermal Properties of the HBFP, Diamine-Terminated PEG, and Crosslinked HBFP-PEG Materials as Dry Samples and Samples Swollen with Water, Determined by DSC, and Decomposition Temperatures of the Same, Determined by TGA^a

Material	PEG (wt %)	Transition Temperature ($^{\circ}$ C, DSC)		TGA	
		Dry Samples	H ₂ O-Swollen Samples ^b	Onset Temperature ($^{\circ}$ C)	Weight Loss (%)
1c	0	55.5	— ^c	337.2	24.1
2a	14	46.8	— ^c	332.7	40.5
2b	29	44.4	-29.2	331.8	57.5
2c	45	47.2	-25.8	349.6	63.6
2d	55	48.2	-23.3	355.9	69.6
PEG-(NH ₂) ₂	100	49.9	-27.3	368.9	96.0

^a The HBFP (**1c**) was used in the preparation of the crosslinked HBFP-PEG materials used in the thermal analysis.

^b Melting transition for the PEG-hydrate complex.

^c Data not obtained.

materials (Table 4). Thermograms of the dry samples, as shown in Figure 6, indicated a T_g for the HBFP at 55.5 °C and a T_m for the diamino-terminated PEG at 49.9 °C.

Each of the hybrid materials exhibited thermal transitions that were characteristic of semicrystalline or crystalline PEG domains, supporting the phase segregation of PEG from the HBFP. In comparison with the amorphous HBFP, **2a** with 14 wt % PEG shows a melting transition ($T_{m,1}$; Fig. 6, inset) at 46.8 °C, indicating a semicrystalline domain. The melting transition endotherm increased in size with an increase in the weight

percentage of PEG to 29% for **2b**. The melting endotherm of Figure 6, for **2c**, revealed two transitions, $T_{m,1}$ and $T_{m,2}$, that were probably due to PEG domains of different crystallinities; that is, the localized PEG domains resulted in a higher T_m , and the domains of PEG in the HBFP-PEG phase continuum resulted in a lower degree of crystallinity. Frey et al.⁷³ observed multiple transitions for esterified hyperbranched polyether polyols that were believed to result from different crystallites. **2d**, with the highest PEG content, exhibited only the higher temperature transition, $T_{m,2}$, and this indicated the predominance of PEG

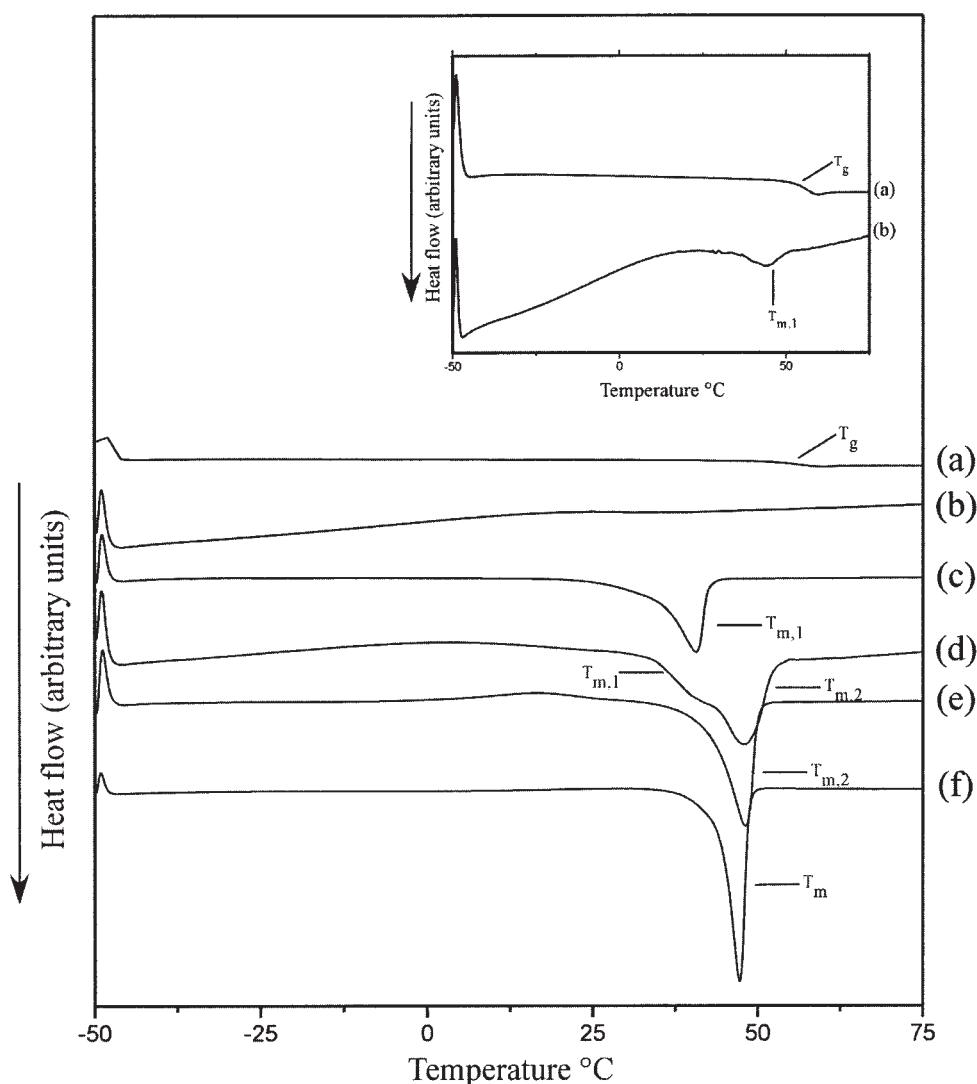


Figure 6. DSC thermograms of (a–e) dry crosslinked HBFP-PEG materials (**1c**, **2a**, **2b**, **2c**, and **2d**, respectively) and (f) diamino-terminated PEG. Increasing the degree of crosslinking results in multiple PEG domains that vary in the degree of crystallinity. The traces shown here are the third heating runs. HBFP **1c** was used in the preparation of these materials.

with higher crystallinity, similar to that of the pure PEG, yet the individual components of PEG and HBFP must have been interspersed throughout the entire insoluble network. On the basis of these results, it can be concluded that the phase-separation process, which depended on the relative compositions of the constituent blocks,⁷⁴ resulted in morphological heterogeneity that was submicroscopically resolved to a greater extent for **2c** with 45 wt % PEG, whereas the coating with 55 wt % PEG (**2d**) consisted of discrete but larger domains of PEG resulting from enhanced PEG chain movement at higher concentrations. All T_m 's were reproducible in several heating and cooling cycles.

With respect to the potential application of the crosslinked HBFP-PEG materials as marine antifouling coatings, it is important to examine the morphologies of these materials in the presence of water, especially because it has been presumed that PEG forms a hydrate complex that is responsible for its resistance toward protein adsorption.^{75,76} For this purpose, DSC was performed on hydrogels prepared by the swelling of samples in a known amount of water (30–40 wt %) for 30 min. As shown in Figure 7, the thermogram for

pure diamino-terminated PEG exhibited two transitions, $T_{m,1}$ at -27.3 °C, which was due to the PEG-hydrate complex, and $T_{m,2}$ at -4.3 °C, which corresponded to free or unbound water. No PEG-hydrate transition was observed for **2a** (not shown in the figure), and the relative amount of water that was engaged in a PEG hydrate increased with an increasing amount of PEG for **2b**, **2c**, and **2d**.

TGA experiments were conducted to evaluate the thermal stabilities of the crosslinked HBFP-PEG materials. The decomposition temperatures of the pure HBFP and the diamino-terminated PEG were 340 and 370 °C, respectively (Fig. 8). The percentage weight loss for PEG was 96%, indicating total decomposition, and that for HBFP was only 24%, indicating the inherent thermal stability of the polymer up to 600 °C. Although the total percentage weight losses for **2a**, **2b**, **2c**, and **2d** followed an increasing trend, as expected, as the amount of PEG increased, the relative percentages of either HBFP or PEG that underwent thermal decomposition could not be ascertained because of overlapping decomposition profiles.

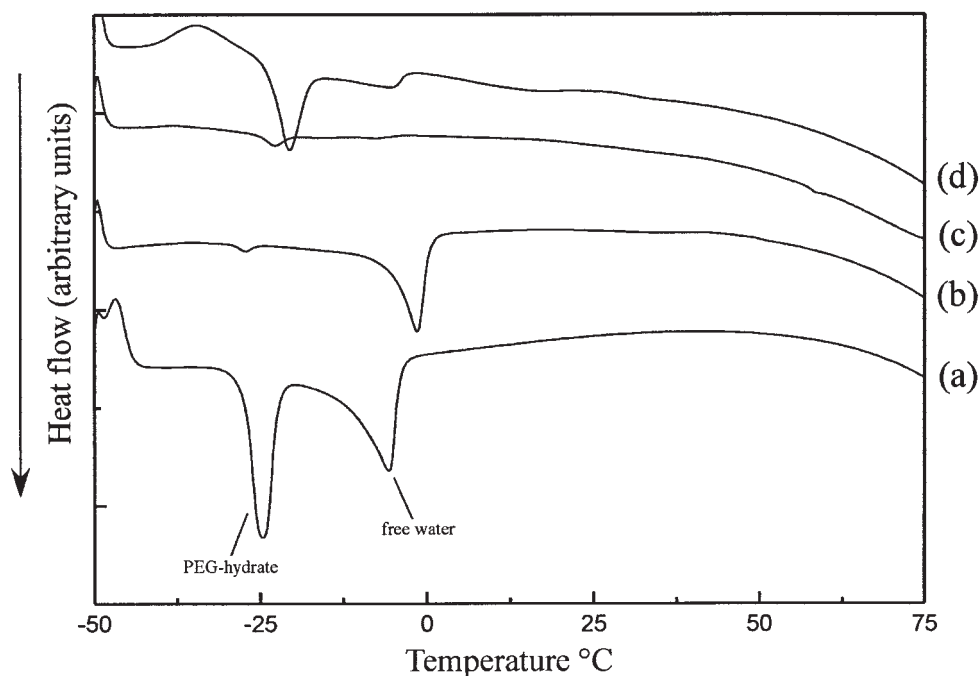


Figure 7. DSC thermograms of hydrogels of the crosslinked HBFP-PEG materials: (a) diamino-terminated PEG, (b) **2b**, (c) **2c**, and (d) **2d**. The PEG-hydrate complex, observed for **2b**, **2c**, and **2d**, increases in size as the PEG composition increases. The traces shown here are the first heating runs. HBFP **1c** was used in the preparation of these materials.

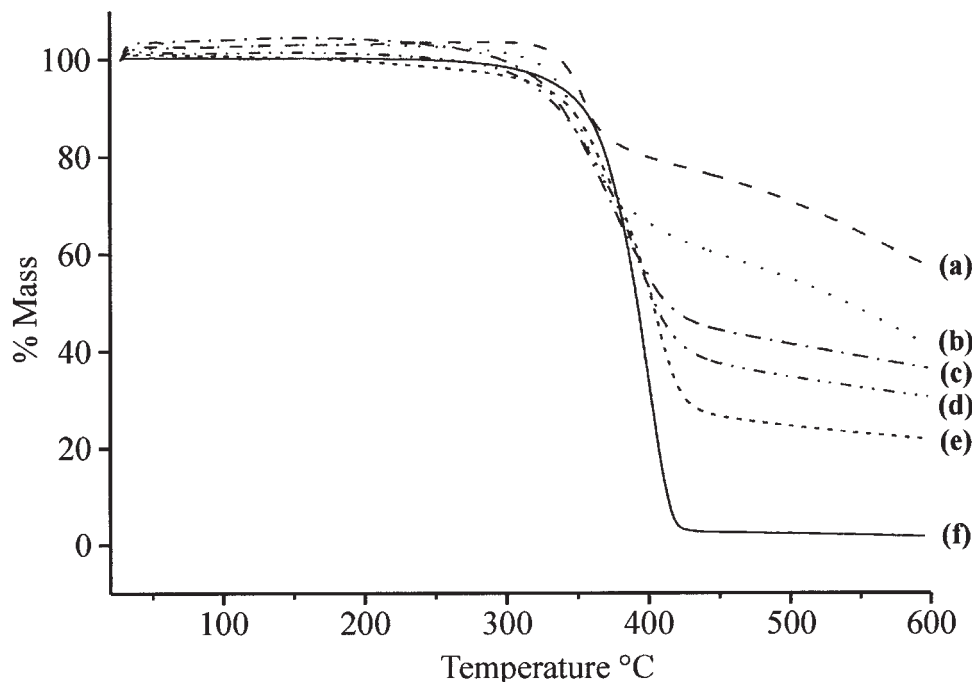


Figure 8. TGA traces of (a–e) crosslinked HBFP–PEG materials (**1c**, **2a**, **2b**, **2c**, and **2d**, respectively) and (f) diamino-terminated PEG. The HBFP was found to be thermally stable up to 600 °C, whereas the relative weight loss increased with an increasing weight percentage of PEG. HBFP **1c** was used in the preparation of the materials used in these experiments.

CONCLUSIONS

Coatings of amphiphilic crosslinked HBFP–PEG networks were prepared on 3-APS-functionalized glass substrates. The static contact-angle values indicated increasing hydrophilicity of the coatings with increasing PEG content at the coating surface, and this was also confirmed by the F/C atomic concentration ratios determined from the XPS experiments. The phase segregation induced by the incompatibility of HBFP and PEG domains was manifested in the AFM and DSC measurements as well, which revealed complex topographical and morphological features that could be manipulated to minimize the interaction of fouling organisms with the surface. The cross-linked networks with 55 wt % PEG possessed the largest discrete PEG domains, as showcased by T_m of the material resembling that of pure PEG. In comparison, the network coating with 45 wt % exhibited multiple T_m 's, unlike any other material in the series, reflecting an inherent morphological heterogeneity that was expected to be expressed, to the same extent, in surface topography and composition as well. We believe that this

level of surface complexity in terms of periodic amphiphilic patterns is essential for a coating to be able to resist the adhesion of biological macromolecules with various affinities toward hydrophobic and hydrophilic surfaces. A quantitative evaluation of the hydrophobic and hydrophilic domains (by small-angle X-ray scattering) and their distributions on a given HBFP–PEG coating (by time-of-flight secondary-ion mass spectrometry) is underway. Other factors that contribute toward fouling resistance behavior, such as the surface free energy and mechanical strength, are also under scrutiny and will be the subject of a subsequent publication.

This material is based on work supported by a contract from the Office of Naval Research (N00014-02-1-0326), which is gratefully acknowledged. The authors also acknowledge Daoji Gan for scientific input during the preliminary phase of this work.

REFERENCES AND NOTES

1. Arnold, M. E.; Nagai, K.; Spontak, R. J.; Freeman, B. D.; Leroux, D.; Betts, D. E.; DeSimone, J. M.;

- DiGiano, F. A.; Stebbins, C. K.; Linton, R. W. *Macromolecules* 2002, 35, 3697.
2. Chapman, T. M.; Benrashid, R.; Marra, K. G.; Keener, J. P. *Macromolecules* 1995, 28, 331.
 3. Schmidt, D. L.; Coburn, C. E.; DeKoven, B. M.; Potter, G. E.; Meyers, G. F.; Fischer, D. A. *Nature* 1994, 368, 39.
 4. Schmidt, D. L.; Coburn, C. E.; DeKoven, B. M.; Potter, G. E.; Meyers, G. F.; Fischer, D. A. *Langmuir* 1994, 12, 518.
 5. Beamson, G.; Alexander, M. R. *Surf Interface Anal* 2004, 36, 323.
 6. Perutz, S.; Wang, J.; Kramer, E. J.; Ober, C. K. *Macromolecules* 1998, 31.
 7. Park, I. J.; Lee, S.; Choi, C. K. *Macromolecules* 1998, 31, 7555.
 8. Fujiwara, H.; Narita, T.; Hamana, H. J. *J Polym Sci Part A: Polym Chem* 2003, 41, 2743.
 9. Lu, Z.; Cheng, L.; Li, J.; Zhang, K.; Yi, S.; Qin, J. *J Polym Sci Part A: Polym Chem* 2004, 42, 925.
 10. Yasutake, M.; Andou, Y.; Hiki, S.; Nishida, H.; Endo, T. *J Polym Sci Part A: Polym Chem* 2004, 42, 2621.
 11. Furukawa, Y.; Yoneda, T. *J Polym Sci Part A: Polym Chem* 2003, 41, 2704.
 12. Hsiao, S.-H.; Chen, W.-T. *J Polym Sci Part A: Polym Chem* 2003, 41, 420.
 13. Hsiao, S.-H.; Yang, C.-P.; Chung, C.-L. *J Polym Sci Part A: Polym Chem* 2003, 41, 2001.
 14. Michel, U.; Resnick, P.; Kipp, B.; DeSimone, J. M. *Macromolecules* 2003, 36, 7107.
 15. Li, K.; Wu, P.; Han, Z. *Polymer* 2002, 43, 4079.
 16. Brady, R. F., Jr.; Bonafede, S. J.; Schmidt, D. L. *Surf Coat Int* 1999, 82, 582.
 17. Youngblood, J. P.; Andruzzi, L.; Ober, C. K.; Hexemer, A.; Kramer, E. J.; Callow, J. A.; Finlay, J. A.; Callow, M. E. *Biofouling* 2003, 19, 91.
 18. Brady, R. F., Jr.; Griffith, J. R.; Love, K. S.; Field, D. E. *J Coat Technol* 1987, 59, 113.
 19. Pullin, R. A.; Nevell, T. G.; Tsibouklis. *Mater Lett* 1999, 39, 142.
 20. Johnston, E.; Bullock, S.; Uilk, J.; Gatenholm, P.; Wynne, K. J. *Macromolecules* 1999, 32, 8173.
 21. Rolland, J. P.; Van Dam, R. M.; Schorzman, D. A.; Quake, S. R.; DeSimone, J. M. *J Am Chem Soc* 2004, 126, 2322.
 22. Pitois, C.; Wiesmann, D.; Lindgren, M.; Hult, A. *Adv Mater* 2001, 13, 1483.
 23. Kostov, G.; Améduri, B.; Boutevin, B.; Bauduin, G.; Stankova, M. *J Polym Sci Part A: Polym Chem* 2004, 42, 1693.
 24. Ito, H.; Okazaki, M.; Miller, D. C. *J Polym Sci Part A: Polym Chem* 2004, 42, 1478.
 25. Naldrett, M. J. *J Mar Biol Assoc* 1993, 73, 689.
 26. Papov, V. V.; Diamonds, T. V.; Biemann, K.; Waite, J. H. *J Biol Chem* 1995, 270, 20183.
 27. Callow, M. *Chem Ind* 1990, 5, 123.
 28. Brady, R. F., Jr. *J Coat Technol* 2000, 72, 44.
 29. Ostuni, E.; Grzybowski, B. A.; Mrksich, M.; Roberts, C. S.; Whitesides, G. M. *Langmuir* 2003, 19, 1861.
 30. Tosatti, S.; De Paul, S. M.; Askendal, A.; Vandevondele, S.; Hubbell, J. A.; Tengvall, P.; Textor, M. *Biomaterials* 2003, 24, 4949.
 31. Wagner, V. E.; Koberstein, J. T.; Bryers, J. D. *Biomaterials* 2004, 25, 2247.
 32. Archambault, J. G.; Brash, J. L. *Colloids Surf B* 2004, 33, 111.
 33. Gouzy, M.-F.; Sperling, C.; Salchert, K.; Pompe, T.; Streller, U.; Uhlmann, P.; Rauwolf, C.; Simon, F.; Bohme, F.; Voit, B.; Werner, C. *Biomaterials* 2004, 25, 3493.
 34. Ko, B. S.; Babcock, B.; Jennings, G. K.; Tilden, S. G.; Peterson, R. R.; Cliffel, D.; Greenbaum, E. *Langmuir* 2004, 20, 4033.
 35. Groll, J.; Amiregoulova, E. V.; Ameringer, T.; Heyes, C. D.; Rocker, C.; Nienhaus, U.; Moller, M. *J Am Chem Soc* 2004, 126, 4234.
 36. Mueller, A.; Kowalewski, T.; Wooley, K. L. *Macromolecules* 1998, 31, 776.
 37. Tomalia, D. A.; Fréchet, J. M. J. *J Polym Sci Part A: Polym Chem* 2002, 40, 2719.
 38. Miller, T. M.; Neenan, T. X.; Kwock, E. W.; Stein, S. M. *J Am Chem Soc* 1993, 115, 356.
 39. Andre, S.; Guida-Pietrasanta, F.; Rousseau, A.; Boutevin, B.; Caporiccio, G. *J Polym Sci Part A: Polym Chem* 2002, 40, 4485.
 40. Gelin, M.-P.; Ameduri, B. *J Polym Sci Part A: Polym Chem* 2003, 41, 160.
 41. Hillmyer, M. A.; Lodge, T. P. *J Polym Sci Part A: Polym Chem* 2002, 40, 1.
 42. Ma, Z.; Lacroix-Desmazes, P. *J Polym Sci Part A: Polym Chem* 2004, 42, 2405.
 43. Fujiwara, T.; Makal, U.; Wynne, K. *Macromolecules* 2003, 36, 9383.
 44. Fréchet, J. M. J. *J Polym Sci Part A: Polym Chem* 2003, 41, 3713.
 45. Guan, Z. *J Polym Sci Part A: Polym Chem* 2003, 41, 3680.
 46. Lecommandoux, S.; Klok, H.-A.; Sayar, M.; Stupp, S. I. *J Polym Sci Part A: Polym Chem* 2003, 41, 3501.
 47. Gitsov, I.; Lambrych, K. R.; Remnant, V. A.; Pracitto, R. *J Polym Sci Part A: Polym Chem* 2000, 38, 2711.
 48. Yin, Y.; Yang, L.; Yoshino, M.; Fang, J.; Tanaka, K.; Kita, H.; Okamoto, K. *J Polym Sci Part A: Polym Chem* 2004, 36, 294.
 49. Yang, H.; Morris, J. J.; Lopina, S. T. *J Colloid Interface Sci* 2004, 273, 148.
 50. Francis, R.; Taton, D.; Logan, J. L.; Masse, P.; Gnanou, Y.; Duran, R. S. *Macromolecules* 2003, 36, 8253.
 51. Gitsov, I.; Fréchet, J. M. J. *J Am Chem Soc* 1996, 118, 3785.

52. Fréchet, J. M. J.; Gitsov, I.; Monteil, T.; Rochat, S.; Sassi, J.-F.; Vergelati, C.; Yu, D. *Chem Mater* 1999, 11, 1267.
53. Johnson, M. A.; Iyer, J.; Hammond, P. T. *Macromolecules* 2004, 37, 2490.
54. Gitsov, I.; Lys, T.; Zhu, C. *Am Chem Soc Symp Series* 2003, 833, 218.
55. Gitsov, I.; Zhu, C. *Macromolecules* 2002, 35, 8418.
56. Gan, D.; Mueller, A.; Wooley, K. L. *J Polym Sci Part A: Polym Chem* 2003, 41, 3531.
57. Gitsov, I.; Zhu, C. *J Am Chem Soc* 2003, 125, 11228.
58. Hexemer, A.; Sivaniah, E.; Kramer, E. J.; Xiang, M.; Li, X.; Fischer, D. A.; Ober, C. K. *J Polym Sci Part B: Polym Phys* 2004, 42, 411.
59. Bertolucci, M.; Galli, G.; Chiellini, E.; Wynne, K. J. *Macromolecules* 2004, 37, 3666.
60. Kingshott, P.; McArthur, S.; Thissen, H.; Castner, D. G.; Griesser, H. J. *Biomaterials* 2002, 23, 4775.
61. Fieldman, K.; Hähner, G.; Spencer, N. D.; Harder, P.; Grunze, M. *J Am Chem Soc* 1999, 121, 10134.
62. Cunliffe, D.; Smart, C. A.; Alexander, C.; Vulfson, E. N. *Appl Environ Microbiol* 1999, 65, 4995.
63. Finlay, J. A.; Callow, M. E.; Ista, L. K.; Lopez, G. P.; Callow, J. A. *Integr Comp Biol* 2002, 42, 1116.
64. Sigal, G. B.; Mrksich, M.; Whitesides, G. M. *J Am Chem Soc* 1998, 120, 3464.
65. Lyubchenko, Y. L.; Gall, A. A.; Shlyakhtenko, L. S. *Methods Mol Biol* 2001, 148, 569.
66. Emoto, K.; Van Alstine, J. M.; Harris, J. *Langmuir* 1998, 14, 2722.
67. Kiss, É.; Samu, J.; Tóth, A.; Bertóti, I. *Langmuir* 1996, 12, 1651.
68. Lovrecich, M.; Rubessa, F. *Pharm Dev Technol* 1998, 3, 123.
69. Mera, A. E.; Goodwin, M.; Pike, J. K.; Wynne, K. J. *Polymer* 1999, 40, 419.
70. Wang, J.; Mao, G.; Ober, C. K.; Kramer, E. J. *Macromolecules* 1997, 30, 1906.
71. Chen, W.; Wu, J.; Jiang, M. *Macromol Chem Phys* 1998, 199, 1683.
72. Hester, J. F.; Banerjee, P.; Won, Y. Y.; Akthakul, A.; Acar, M. H.; Mayes, A. M. *Macromolecules* 2002, 35, 7652.
73. Sunder, A.; Bauer, T.; Mulhaupt, R.; Frey, H. *Macromolecules* 2000, 33, 1330.
74. Jang, J.; Oh, J. H.; Moon, S. I. *Macromolecules* 2000, 33, 1864.
75. Jeon, S. I.; Andrade, J. D. *J Colloid Interface Sci* 1991, 142, 159.
76. Jeon, S. I.; Lee, L. H.; Andrade, J. D.; de Gennes, P. G. *J Colloid Interface Sci* 1991, 142, 149.